Naval Research Laboratory
Washington, DC 20375-5320

NRL/MR/4404—92-7106

Mixing Regimes in a Spatially Confined, Two-Dimensional, Supersonic Shear Layer

P. VUILLERMOZ

ONERA and Société Européenne de Propulsion
France

AND

E. S. ORAN

Laboratory for Computational Physics and Fluid Dynamics

July 31, 1992

REPORT DOCUMENTATION PAGE

Form Approved
OMB No 0704-0188

1. AGENCY USE ONLY (Leave blank)	2. REPORT DATE	3. REPORT TYPE AND DATES COVERED
	July 31, 1992	Interim

4. TITLE AND SUBTITLE
Mixing Regimes in a Spatially Confined, Two-Dimensional, Supersonic Shear Layer

5. FUNDING NUMBERS
61102F
DN150-096

6. AUTHOR(S)
P. Vuillermoz* and E.S. Oran

7. PERFORMING ORGANIZATION NAME(S) AND ADDRESS(ES)
Naval Research Laboratory
Washington, DC 20375-5320

8. PERFORMING ORGANIZATION REPORT NUMBER
NRL/MR/4404—92-7016

9. SPONSORING / MONITORING AGENCY NAME(S) AND ADDRESS(ES)
AF Office of Scientific Res
Bolling AFB, Washington, DC 20332

Office of Naval Research
Arlington, VA 22217-5999

10. SPONSORING / MONITORING AGENCY REPORT NUMBER

11. SUPPLEMENTARY NOTES
*On leave from ONERA and sponsored by Société Européenne de Propulsion, France.

12a. DISTRIBUTION / AVAILABILITY STATEMENT
Approved for public release; distribution unlimited.

12b. DISTRIBUTION CODE

13. ABSTRACT *(Maximum 200 words)*

The evolution of a high-speed, compressible, confined, temporally evolving supersonic mixing layer between hydrogen and oxygen gas streams is examined using time-dependent, two-dimensional, numerical simulations that include the effects of viscosity, molecular diffusion, and thermal conduction. The flow shows three distinct mixing regimes: an apparently ordered, laminar stage in which the structures grow due to the initial perturbation; a convective-mixing regimes in which vortices begin to interact and structures grow; and a diffusive-mixing regime in which vortical structures break down and diffusive mixing dominates. Varying the strength of the diffusion terms shows that these effects are important in the laminar and diffusive-mixing stages, but not in the convective mixing stage. Varying the convective Mach shows that compressibility does not change the general structural features of the mixing process, although higher compressibility results in a slower transition between the various flow regimes. Increasing the size of the computational domain increases the absolute time of transition from convective to diffusive mixing, but does not affect the dimensionless time normalized to the system size.

14. SUBJECT TERMS
Mixing regimes
Supersonic shear layer
Hydrogen and oxygen reactions

15. NUMBER OF PAGES
41

16. PRICE CODE

17. SECURITY CLASSIFICATION OF REPORT	18. SECURITY CLASSIFICATION OF THIS PAGE	19. SECURITY CLASSIFICATION OF ABSTRACT	20. LIMITATION OF ABSTRACT
UNCLASSIFIED	UNCLASSIFIED	UNCLASSIFIED	UL

NSN 7540-01-280-5500

Standard Form 298 (Rev 2-89)
Prescribed by ANSI Std 239-18
298-102

CONTENTS

MIXING REGIMES IN A SPATIALLY CONFINED, TWO-DIMENSIONAL, SUPERSONIC SHEAR LAYER

Introduction

The successful design of propulsive engines for hypersonic vehicles requires accurate prediction of the mixing and combustion efficiency in high-speed flows. In order to achieve this predictive capability, we need an improved understanding of the dominant processes. One way to obtain this understanding when there are many complex interacting physical processes and the interactions are highly nonlinear is to use numerical methods to simulate the flow, a use to which simulations are well suited in the sense that they can extend the theoretical analyses of idealized systems and the processes evaluated can usually be included or not in a controlled manner. However, now we are now faced with the situation where the simulations are not only being used to study the fundamental processes, but are also being used to evaluate and design supersonic and hypersonic propulsion systems, even thought there remain a number of questions concerning the simulations and the effects of various physical processes that are not completely understood. In this paper, we address certain fundamental physical questions about the effects of viscosity, molecular diffusion, and compressibility through the evolution of a high-speed mixing layer.

Since the Brown and Roshko[1] observations, many experimental studies have confirmed the existence of large-scale coherent structures in mixing layers for both high and low Reynolds numbers. These structures arise initially from the Kelvin-Helmholtz instabilities and they move downstream within the layer with a convective velocity U_c. Bogdanoff[2] and Roshko and Papamoshou[3] have given approximations of this velocity based on the assumption that there is a stagnation point in the center of each coherent structure and that the flow comes to rest isentropically at the stagnation point. When the ratio of specific heats γ is identical for each gas, Roshko and Papamoshou conclude that the relative Mach numbers, M_{c_1} and M_{c_2}, between the structures and each stream must be equal. That is,

$$M_{c_1} = M_{c_2} \equiv M_c \qquad \text{with } M_{c_1} = \frac{U_c - U_1}{a_1} \text{ and } M_{c_2} = \frac{U_2 - U_c}{a_2}, \tag{1}$$

where a_1 and a_2 are the speeds of sound for the streams 1 and 2, respectively. This analysis allows us to evaluate U_c,

$$U_c = \frac{(a_1 U_2 + a_2 U_1)}{(a_1 + a_2)}. \tag{2}$$

The quantities M_c and U_c are useful for characterizing the flow properties and will be used throughout this paper.

There has been a large body of experimental work describing these structures since the early work of Brown and Roshko. Papamoschou and Roshko[3] showed the effects of

Manuscript approved May 21, 1992.

compressibility on the growth of the shear layer, and recently, Dimotakis[4] summarized experiments on the entrainment process and structure in subsonic shear layers. Other important recent experiments aimed at isolating the effects of compressibility on the flow structures have been performed by Clemens et al.[5], who showed that there did not appear to be any organized structures forming for M_c more than 0.6, and Samimy and Elliot[6] who showed that the mixing level decreases when M_c increases. Whereas the experiments by Dahm et al.[7] have focused on the structure of mixing in incompressible liquid jets, the small-scale structures that they see might be a general property of fully developed mixing layers.

There are two different theoretical approaches to studying the development of a mixing layer between two parallel isobaric streams with differing velocities. One is to consider the *spatially evolving mixing layer*, which considers the problem in the laboratory frame of reference and observes the growth of the shear layer from the initial point of interaction up to the outflow boundary. The second approach is the *temporally evolving mixing layer*, which is an attempt to consider the system in a frame of reference moving with the large-scale structures considers the boundary conditions as periodic. The spatially evolving problem is in fact the more physically realistic problem although it has the difficultly of requiring the specification of inflow and outflow boundary conditions.

There have been a number of theoretical stability analyses and concommitant numerical simulations of both spatially and temporally evolving shear layers. Metcalfe et al.[8] focussed on the incompressible mixing layer. Ragab and Wu[9] and Jackson and Grosch[10] have shown that for high M_c. there are several unstable modes and three-dimensional modes become important. Numerical simulations have used spectral and vortex methods, mostly for incompressible flows, and finite-difference and finite-volume methods for incompressible and incompressible flows. Using spectral methods, Riley and Metcalfe[11] have performed low Reynolds number direct numerical simulations of incompressible flows, and McMurtry et al.[12] have considered the effects of heat-release on the large-scale structures. Sandham and Reynolds[13] have considered two-dimensional and three-dimensional stability analysis and compared these to simulations, as have Lele[14] and Ragab and Sheen.[15] Lele has considered both temporally and spatially evolving flows where the same species is on both sides of the mixing layer. Using vortex-dynamics methods, Soteriou et al.[16] considered the effects of density gradients. Ragab and Sheen[15] used a high-order finite-volume method to compute the growth rates of unstable modes of a supersonic shear layer, and they have

compared these to the predictions of linear stability theory. In addition, they have compared the results of large-eddy simulations to direct numerical simulations and examined the effects of the numerical diffusion on the spectrum. Guirguis et al.[17] and Farouk et al.[18] have studied spatially evolving mixing layers for equal pressure, underexpanded, and overexpanded systems.

In this paper, we focus on the mixing of streams of hydrogen and oxygen, so that we are studying the features of a high-speed, compressible shear between two gases of very different densities and thermophysical properties. These simulations use correct, unscaled values of the physical diffusion parameters such as viscosity, thermal conduction, and molecular diffusion, and thus allow us to evaluate the effects of these on a variety of diagnostic parameters of the flow. For example, we have parametrically varied the size or presence of various diffusion effects, the compressibility through the convective Mach number, and the absolute size of the system. To eliminate some of the physical complexity inherent in simulating inflow and outflow boundary conditions, we confine this study to a bounded, temporally evolving mixing layer. With this approach, we can examine the growth and decay of the mixing process and we can also point out the effects of various physical processes and approximations.

Physical and Numerical Model

General Formulation

We solve the time-dependent, two-dimensional, compressible, Navier-Stokes equations for a multispecies gas, including the effects of molecular diffusion and thermal conduction. The balance equations for the densities, momentum, and energy are

$$\frac{\partial \rho}{\partial t} = -\nabla \cdot (\rho \mathbf{v}) , \tag{3}$$

$$\frac{\partial n_i}{\partial t} = -\nabla \cdot (n_i \mathbf{v}) - \nabla \cdot (n_i \mathbf{v}_{di}) \qquad i = 1, ..., N_s , \tag{4}$$

$$\frac{\partial \rho \mathbf{v}}{\partial t} = -\nabla \cdot (\rho \mathbf{v}\mathbf{v}) - \nabla \cdot \mathbf{P} , \tag{5}$$

$$\frac{\partial E}{\partial t} = -\nabla \cdot (E\mathbf{v}) - \nabla \cdot (\mathbf{v} \cdot \mathbf{P}) - \nabla \cdot \mathbf{q} , \tag{6}$$

where n_i is the number density for the species i. The mass fraction of species i is Y_i, defined by

$$n_i = \frac{\rho Y_i}{W_i} , \tag{7}$$

where W_i is the molecular weight, and the total number density is

$$N = \sum_i n_i = \sum_i \frac{\rho Y_i}{W_i} . \tag{8}$$

We assume an ideal-gas equation of state,

$$P = \rho \frac{R_0}{W} T , \tag{9}$$

where the molecular weight of the mixture is given by

$$\frac{1}{W} = \sum_i \frac{Y_i}{W_i} . \tag{10}$$

The auxiliary equation for pressure $\mathbf{P}$ and heat conductive flux $\mathbf{q}$ are

$$\mathbf{P} \equiv P(N,T)\,\mathbf{I} + \frac{2}{3}\mu_m(\nabla \cdot \mathbf{v})\,\mathbf{I} - \mu_m[(\nabla \mathbf{v}) + (\nabla \mathbf{v})^T] \tag{11}$$

and

$$\mathbf{q} = -\lambda_m \nabla T + \rho \sum_i h_i Y_i \mathbf{v}_{di} . \tag{12}$$

The specific enthalpy h_i can be written as

$$h_i = \int_0^T C_{p_i} dT + h_{i_0} , \tag{13}$$

where C_{p_i} and h_{i_0} are the specific heat at constant pressure and heat of formation of species i, respectively. We neglect the radiative fluxes and the Soret and Dufour effects (thermal diffusion), which can be justified because radiative fluxes for hydrogen gases are negligible and the temperature gradients remain small.

Diffusion Model

The diffusion velocities $\mathbf{v}_{di}$ are solutions of the following system of equations (see, for example, Oran and Boris[19]),

$$\nabla X_i = \sum_j \frac{X_i X_j}{D_{ij}} (\mathbf{v}_{dj} - \mathbf{v}_{di}) + (Y_i - X_i) \left(\frac{\nabla P}{P} \right) , \tag{14}$$

where, for each species i, X_i is the mole fraction, $\mathbf{v}_{di}$ the diffusion velocity, and D_{ij} the diffusivity of the species i into the species j.

These diffusion velocities must obey to the condition of mass conservation such that

$$\sum_i Y_i \mathbf{v}_{di} = \mathbf{0} . \tag{15}$$

Here, we approximate the solution of the system of equations (14) and (15) by a gradient law, as proposed by Coffee and Heimerl,[20]

$$\hat{\mathbf{v}}_{di} = -\frac{1}{X_i} D_i^m \nabla X_i \qquad D_i^m = \frac{1 - Y_i}{\sum_{j \neq i} X_j / D_{ij}} . \tag{16}$$

Then we correct these velocities in order to insure the mass conservation, equation (15),

$$\mathbf{v}_c = -\sum_j Y_j \hat{\mathbf{v}}_{dj} \tag{17}$$

and

$$\mathbf{v}_{di} = \hat{\mathbf{v}}_{di} + \mathbf{v}_c . \tag{18}$$

This approximation becomes rigorously correct in the binary case.

The mixture thermal conductivity λ_m and viscosity μ_m are computed from the conductivity λ_i and molecular viscosity μ_i of the individual gases. The $\{\lambda_i\}$, $\{\mu_i\}$, and binary diffusion coefficients $\{D_{ij}\}$ are expressed as polynomial functions of the temperature.[19]

Numerical Integration

The convection is solved using a standard Flux-Corrected Transport (FCT) algorithm, LCPFCT.[21] This is a nonlinear, monotone algorithm that is fourth-order accurate in phase. The integration is carried out by a two-step predictor-corrector procedure with, successively, a diffusive and anti-diffusive step. The first step modifies the linear properties of a high-order algorithm by adding diffusion during convective transport to prevent dispersive ripples from arising. The added diffusion is removed in an antidiffusion step. The result is that the calculations maintain the high order of accuracy without requiring artificial viscosity to stabilize them. The algorithm has been tested and used extensively in the last fifteen years (see, for example, bibliography Reference 19) to predict a wide variety of flows. Recently it has been used to investigate unstable spatially evolving supersonic flows.[17,18] and compared computations to the results of comparisons of growth rates of linear instabilities[18] to those predicted by linear stability analyses.[15]

The physical diffusion terms are solved in conservative finite-volume form by second-order centered algorithms.[22] More specifically, we use the values of the diffusive fluxes at the interfaces between the grid nodes. Their expressions are obtained from first-order centered approximations of the primary variables.[19] An overall global timestep Δt is chosen by evaluating a stability criterion for each type of term and then selecting the minimum of

these for Δt. During a computational timestep Δt, each process is integrated for the time interval Δt using the most recent values of the variables.[19]

The Model Problems

Here we define two problems. The first is a one-dimensional problem used to obtain self-consistent initial conditions across the shear layer. The solution of this problem provides self-consistent initial conditions for the second problem, the two-dimensional shear layer.

The One-Dimensional Problem

Starting from a step profile for each variable in the y direction, we compute the evolution of a mixing layer between two gases by solving the full set of equations (3) - (6), and assuming that there are no variations along the x direction,

$$\frac{\partial \varphi}{\partial x} = 0 . \tag{19}$$

Here φ represents ρ, $\rho \mathbf{v}$, $\{n_i\}$, and E. The boundaries at the bottom and the top of the domain are open, which means that $\partial\varphi/\partial y = 0$ when $y = \pm H$. These boundary conditions are used to avoid the reflection of the transient waves generated as the singular initial condition equilibrates. The solution shows how the pressure equilibrates in the vertical direction and thus provides self-consistent initial conditions for the fluid and individual species profiles.

The Two-Dimensional Problem

The two-dimensional computational domain, shown schematically in Figure 1, consists of a rectangle of length L and height $H = L/2$. The left and right boundaries are periodic, which means that $\varphi(0, y) = \varphi(L, y)$, and the bottom and top boundaries are slip wall conditions, $\rho v_y = 0$ and $\partial\varphi/\partial y = 0$ where $\varphi = \{\rho, \rho v_x, \{n_i\}, E\}$ at $y = 0$ and $y = H$. The computational cell size is always kept uniform in the x and y directions and are in the range $\Delta x = \Delta y = (2.5 - 10) \times 10^{-5}$ m, so that the timesteps are in the range $(2 - 8) \times 10^{-3}$ μs. A typical computation described below requires about 10,000 timesteps. For each case, we evaluated the effects of viscosity and diffusion by comparing the solutions of the complete set of equations (3) - (6) (referred to as NS+) that contain heat conduction, molecular diffusion, convection, and viscosity, to the Euler solutions obtained from solving only the convective transport equations.

Mixing and Flow Diagnostics

A well known feature of homogenous incompressible turbulence is the energy cascade from the large scales to the small scales (Taylor or Kolmogorov) where the convective energy is converted to internal energy. In three dimensions, this transfer is accomplished by stretching of the vorticity field, $\omega = \nabla \times \mathbf{v}$, a property that appears from the term in the vorticity equations of the form $(\omega \cdot \nabla)\mathbf{v}$. For two-dimensions, the vorticity is no longer subject to this effect and becomes a conservative variable. The early works of Batchelor[23] and more recently Lesieur[24] showed that for the two-dimensional case, we may use the enstrophy, ω^2, to describe the flow. This variable has properties similar to vorticity for three-dimensional turbulence, that is, there is a cascade process, independent of the viscosity, to higher wavenumbers where the enstrophy is dissipated.

In order to examine the global intensity of the flow, we define a parameter M_ω such that

$$M_\omega = \left(\frac{1}{<\omega^2>}\right)^{\frac{1}{2}} \tag{20}$$

where $<>$ indicates the average taken on the computational domain. In the particular case of an incompressible, homogeneous flow, Batchelor showed that M_ω is a linear function of time.

The mixing of the different gases can be described in terms of the area S^m of the computational domain where the fraction of both gases is neither exactly zero nor exactly one. We can estimate the value of S^m from the mass fraction, Y_i, or mole fraction, X_i. For example, for a binary mixture,

$$S_Y^m \equiv 4\int\int Y_1\, Y_2 dxdy = 4\int\int Y_1\,(1-Y_1)dxdy \tag{21}$$

$$S_X^m \equiv 4\int\int X_1\, X_2 dxdy = 4\int\int X_1\,(1-X_1)dxdy\,, \tag{22}$$

where $Y(1-Y)$ and $X(1-X)$ reach a maximum value when the mixture is completely mixed, that is, when the mass fractions $Y_1 = Y_2 = 0.5$ or the mole fractions $X_1 = X_2 = 0.5$. We consider both spatial averages of these quantites over the computational domain and the instantaneous contours. It is useful to define two global paramaters, M_X and M_Y, such that

$$M_X = \frac{S_X^m}{S_{tot}} \qquad M_Y = \frac{S_Y^m}{S_{tot}}\,, \tag{23}$$

where S_{tot} is the total surface of the entire computational domain, $L \times H$. These parameters evolve between the values 0 and 1.

We can determine the final composition of the mixture obtained from two streams of species 1 and 2 when the time elapsed is long enough to obtain a homogeneous scalar field. The two-dimensional domain does not have any external inflow or outflow and therefore the integrated value of a conservative variable $\int\int \varphi \, dx \, dy$ is constant. Applying this condition for n_1 and n_2 gives the final values n_1^∞ and n_2^∞,

$$n_1^\infty = \frac{1}{2} n_1^0 \quad \text{and} \quad n_2^\infty = \frac{1}{2} n_2^0 \,, \tag{24}$$

which gives

$$X_1^\infty = X_2^\infty = 0.5 \quad \text{and} \quad Y_1^\infty = \frac{W_1}{(W_1 + W_2)} \,, \; Y_2^\infty = \frac{W_2}{(W_1 + W_2)} \,. \tag{25}$$

This allows us to assess the theoretical limits of M_X^∞ and M_Y^∞,

$$M_X^\infty = 1 \qquad \text{and} \quad M_Y^\infty = 4 \frac{W_1 W_2}{(W_1 + W_2)^2} \,, \tag{26}$$

where for the hydrogen and oxygen mixture considered, $M_Y^\infty = 0.22$. Finally, the quantity $M_{\nabla Y}$ is defined as

$$M_{\nabla Y} = < \nabla Y_{H_2} \nabla Y_{H_2} > \,, \tag{27}$$

which is related to the dissipation of scalar energy in the computational domain.

The One-Dimensional Problem

When there is only one species present, there is a closed-form similarity solution that describes the steady-state one-dimensional, incompressible solution across the shear layer. Thus a two-dimensional computation may be intialized with this solution for a finite-thickness shear layer. Because such a closed-form initialization does not exist for a compressible, multispecies problem, it was necessary to develop a procedure for finding finite-thickness, one-dimensional profiles for multispecies problems.

One-Dimensional Validation

First consider a one-dimensional shear layer in the incompressible flow regime (that is, the low Mach number regime), in which the are two streams with the same molecular weight, denoted 1 and 2 . This configuration may be described by a self-similar solution that can be obtained by solving equations (3) – (5) for the mass, the number densities, and the momentum. Moreover, under the previous assumption of constant density and

with equation (19), the condition of zero gradient in the longitudinal direction, the mass conservation equation is reduced to $v_y = 0$. Then equations (4) and (5) can be written

$$\frac{\partial v_x}{\partial t} = \nu \frac{\partial^2 v_x}{\partial y^2}, \quad \frac{\partial Y_i}{\partial t} = D_{12} \frac{\partial^2 Y_i}{\partial y^2} \tag{28}$$

where $\nu = \mu_m/\rho$. We solve this equation by introducing a similarity variable,

$$\eta = \frac{y}{\sqrt{\nu t}}, \tag{29}$$

which leads to

$$\frac{(v_x - U_1)}{(U_2 - U_1)} = \frac{1}{\sqrt{\pi}} \int_{-\infty}^{\eta} e^{-\frac{1}{4}\eta^2} d\eta, \quad Y_2 = \frac{1}{\sqrt{\pi}} \int_{-\infty}^{\eta} e^{-\frac{1}{4S_c}\eta^2} d\eta \tag{30}$$

where $S_c = \nu/D_{12}$. This expression allows us to compute the evolution of the parameter M_ω as a function of time. The final result is

$$M_\omega \sim (\nu t)^{\frac{1}{4}}. \tag{31}$$

Figures 2a and 2b shows the numerically computed, instantaneous, one-dimensional profiles of n_{H_2} and v_x for a problem in which $M_c = 0.01$. The initial profiles of the variables are step functions across the shear line and the computations show that in time, the solutions approach a steady value. Figures 2c and d, which compare the analytical solution to these profiles collapsed as a function of η, shows that the numerical solution is self-similar and that there is reasonable agreement between the incompressible theory and the computed results for a low-velocity, compressible flow problem.

One-Dimensional Mixing Layer

Now consider a one-dimensional problem where one stream is molecular hydrogen and the other is molecular oxygen. The problem is initialized with a discontinuity in all the physical variables between the two streams of opposite Mach number, except for the temperature, which is constant across the streams. We are interested in obtaining the self-consistent steady-state solution to use to initialize the two-dimensional problem.

Figure 3, which shows several instantaneous profiles of n_{H_2} and v_x as functions of y and η (equation (29)) for a case where $M_c = 0.6$, shows that the solution is still self-similar, as is the case for the incompressible one-dimensional shear layer. This self-similarity is characteristic of flows such as mixing layers that do not have any particular length scale.[13] Figure 4 shows how this mixing layer develops in time for the parameters, $Y_{H_2}(1 - Y_{H_2})$,

$X_{H_2}(1 - X_{H_2})$, M_X, and M_Y. When the interface decays, M_X remains at its maximum value in the well mixed regions while M_Y falls as quickly as Y_{H_2}. The temporal evolution of $< M_X >$ is monotonic, but $< M_Y >$ increases to a maximum and then decreases when the interface decays. Note that M_ω (not shown here) evolves as $t^{1/4}$ as predicted by the analytical solution, equation (31) and, as the interface decays, the evolution of M_ω becomes linear.

The Two-Dimensional Problem

In the two-dimensional studies of a mixing layer that develops between a stream of hydrogen and oxygen at the same initial pressure and temperature, the initial unperturbed conditions are taken from the one-dimensional calculations. The instability is initiated by perturbing the finite-thickness layer by superimposing a set of harmonic and subharmonic disturbances on the initial pressure field P_0,

$$P = P_0 \times \left[1 + \alpha \cos(\Omega x) + 0.5\, \alpha \cos\left(\frac{\Omega}{2} x\right)\right] \tag{32}$$

with $\alpha = 0.05 \exp(-y^2/\delta_o^2)$, where δ_o is the initial thickness of the layer and $\Omega = 2\pi/\Lambda$ specifies the harmonic perturbation. A perturbation similar to this for intializing an incompressible mixing layer was used by Metcalfe et al.[8] In the calculations presented below, we have chosen δ_o and the instability wavelength such that $\delta_o/L = 1/50$ and $\Lambda/L = 1/4$.

Dimensionless Numbers and Characteristic Scales

A significant feature of this flow is the wide range of its energy spectrum. The largest scales may be characterized by a length l and a velocity U, and the smallest dissipative scales may be characterized by a length η and velocity u. If we assume that there is an equilibrium between the convection and the dissipation of energy, we can compare the large and small scales. This assumption means that the characteristic time t_c of the transport of energy by the large eddies is equal to the times t_v and t_d of its dissipation by viscosity or diffusion, $t_c = t_v = t_d$, where

$$t_c = \frac{l}{U} \tag{33}$$

and

$$t_v = \frac{U^2}{\epsilon_t} \quad \text{and} \quad t_d = \frac{1}{\epsilon_Y}\,. \tag{34}$$

Here ϵ_t is the dissipation of kinetic energy, $k = \frac{1}{2} < U'^2 >$, and ϵ_Y is the dissipation of scalar energy, $\frac{1}{2} < Y'^2 >$, which may be written as

$$\epsilon_t = \frac{\mu}{\rho} < \mathbf{S}'\mathbf{S}' > = \frac{\mu}{\rho \tau^2} \tag{35}$$

and

$$\epsilon_Y = D < \nabla Y' \nabla Y' > = \frac{D}{\eta_Y^2} , \tag{36}$$

where η_Y is the mixing scale, $\mathbf{S}$ is the tensor of deformation,

$$\mathbf{S} = \frac{2}{3}(\nabla \cdot \mathbf{v})\,\mathbf{I} - |(\nabla \mathbf{v}) + (\nabla \mathbf{v})^T|$$

and $\tau = \eta/u$. Note that the prime indicates fluctuation of the variable.

Defining the Kolmogorov scale η_k as that scale where the molecular viscosity transforms the kinetic energy into heat (that is, the scale at which the Reynolds number is of order unity, $Re_k = \rho \eta_k u/\mu \sim 1$), gives

$$\frac{\eta_k}{l} = Re^{-\frac{3}{4}} , \tag{37}$$

where $Re = \rho l U/\mu$ is the Reynolds number of the large scale.

In the same way, the equilibrium condition allows us to evaluate η_Y,

$$\frac{\eta_Y}{l} = P_e^{-\frac{1}{2}} , \tag{38}$$

where P_e is the Peclet number such that $P_e = lU/D = S_c\, Re$ and $S_c = \mu/\rho D$ is the Schmidt number. When $S_c = 1$, η_Y is the Taylor scale.

Tables 1 and 2 show relevant coefficients, dimensionless numbers, and characteristic scales for the hydrogen-oxygen problem we are considering for a temperature of 500 K and static pressure of 3.5×10^4 Pa. The Prandtl, Schmidt, and Lewis numbers are calculated from $Pr = \mu Cp/\lambda$, $Sc = \mu/\rho D$, $Le = Sc/Pr$, respectively. The values of l and U characterizing the largest scales are taken as $l \sim H$ where H is the system size and $U \sim (U_2 - U_1) = M_c(a_1 + a_2)$, respectively. The Reynolds number of the large scale is then $Re = \rho U l/\mu \sim [\rho_1 a_1/\mu_1 + \rho_2 a_2/\mu_2] M_c H$. The Kolmogorov scale η_k and mixing scale η_Y are evaluated using equations (37) and (38).

Discussion and Analysis of Mixing Regimes

Figure 5 shows the evolution of four global parameters, the quantities M_X, M_Y, M_ω, and $M_{\nabla Y}$ evaluated during the course of a two-dimensional calculation for the base case of convective Mach number $M_c = 0.6$ for the full NS+ calculation. They are shown as a function of a dimensionless time defined by dividing the real time t by an estimate t_0 of the convective time scale t_c, where

$$t_0 = \frac{H}{M_c(a_1 + a_2)} = H/\Delta U . \tag{39}$$

Note that we begin the computation with a thickness δ_i such that $\delta_i/H = 1/25$, and we keep this ratio constant for all of the computations. Therefore, the convective time scales based on either δ_i or H are equivalent.

The shapes of the curves of M_X and M_Y are similar to those obtained in the one-dimensional calculation, but the mixing is enhanced by at least two orders of magnitude due to convection. The M_Y and $M_{\nabla Y}$ show that there are three stages in the mixing procedure. In the initial growth stage, a laminar growth stage extending to about $t/t_0 \sim 2$, the large structures grow as a consequence of the initial perturbation on the flowfield. The large vortices roll up and grow almost independently of each other. In the first mixing stage extending to about $t/t_0 \sim 5$, which we call the convective-mixing stage, the vortices begin to interact with each other and convective mixing dominates. Mixing occurs as these structures merge and grow and the interfaces between the oxygen and hydrogen stretch and deform. The generation of stretched interfaces corresponds to a sharp growth in the intensity of the scalar dissipation $M_{\nabla Y}$. Finally, there is the stage that occurs when the widths of the interfaces reach the order of magnitude of η_Y and they are destroyed by molecular diffusion. The $M_{\nabla Y}$ drops very quickly, M_Y relaxes to its asymptotic value (0.22) shown in equation (26), and M_ω linearly increases, as predicted for homogeneous turbulence.

Figure 6 shows a series of instantaneous profiles of the mole fraction of hydrogen, Y_{H_2}, during the evolution of the mixing layer. In particular, we note the apparent change from a very regular structure to the extremely mixed structure at the end of the computation. At time t_4 in Figure 6, we see the shear layer expanding towards the lighter fluid on the bottom, an effect noted in the subsonic computations.[16] In most previous subsonic, two-dimensional shear-layer computations and most short-duration three-dimensional simulations, we have not seen the breakdown to the diffusive-mixing regime, but only continued merging and growth of the initial structure. In this highly compressible, supersonic shear flow with wall boundaries, we are able to see this regime due to the perturbations on the large structure causing intense fluctuations and subsequent breakdown. This was also noted in spatially evolving simulations of highly compressible flows.[17,18]

The Effects of Viscosity and Molecular Diffusion

One way to understand the effects of viscosity and diffusion is by considering diagnostics such as those shown in Figure 7 which compares the evolution of M_Y when the Reynolds

and Peclet numbers are finite (NS+ computation) or quasi-infinite (Euler computation). The results shown are for a case with for $M_c = 0.6$. From this computation and similar tests using other parameters, we found that the transition between the two mixing stages does not depend on whether or not we include the viscosity or the diffusion and this transition occurs at the same dimensionless time, indicating that it is only a function of the large-scale convection. There is a significant difference in the diffusive-mixing regime and the full NS+ calculation reaches the final homogeneous state much faster than the inviscid calculation. The local scalar energy dissipation during the diffusive-mixing stage, shown in Figure 8, confirms the existence the layer-like structure of these mixing interfaces and shows that the viscosity and diffusion control mixing in this regime. This kind of observation has been made previously for scalar measurements in incompressible jets.[7]

In order to isolate and examine the effects of molecular diffusion, we compare three NS+ calculations at the same Reynolds number but with different values of Peclet number. The molecular diffusion is turned off completely, the actual, physical values of diffusion coefficients were used (as in the previous computations), or the physical values were multiplied by two. The result of the comparison is presented in Figure 9. The first observation is that the enstrophy parameter is not much affected by varying the diffusion when viscosity is kept constant. There are some phase differences, but the trends are the same. In the laminar stage, the molecular mixing is affected strongly by the diffusion and increases as the diffusion is increased. The initial conditions of the convective-mixing stage are thus determined by the result at the end of the laminar stage, but the convective-mixing process itself is so strong that it erases the memory of the initial condition. However, the final stage is the one in which diffusion is most important and determines the dissipation rate.

It helps now to consider two parameters, the mean length of an interface in the domain, l_i, and mean width of a structure in the domain, δ_i, which we can estimate from

$$M_\chi = \frac{\delta_i l_i}{S_{tot}} \tag{40}$$

and

$$M_{\nabla Y} = \frac{l_i}{\delta_i} \tag{41}$$

which assumes that $\nabla Y_{H_2} \sim 1/\delta_i$. Figure 10 shows how the quantities l_i and δ_i behave as the diffusion coefficients are varied and so provide more understanding of the differences in the diffusion-coefficient comparisons. Note that δ_i does not change much until the diffusive-mixing stage where there is a large increase in width of the structure for the highest diffusion

coefficient. During the diffusive mixing stage, the destruction of the large scales is controlled by the amount of molecular diffusion, determined by the diffusion coefficient.

The Effect of Compressibility

We have performed computations for a range of convective Mach numbers and compared the evolution of the global parameters as a function of dimensionless time, t/t_0. Here the difficulty is to compare the mixing efficiency in a common reference frame for the different cases because the spatial growth of the mixing layer is a function of both the temporal growth of the structures and their mean convective speed, U_c. If we assume that the slow stream always has the same velocity U_1 and that U_1 can be set to zero, we note from equations (1) and (2) that

$$M_c = \frac{U_c}{a_1} \quad \text{and} \quad t_0 \sim \frac{1}{U_c} . \tag{42}$$

Thus for each of the diagnostics, which we designate here as F, where $F = M_\omega$, $M_{\nabla Y}$, M_X, and M_Y,

$$\frac{dF}{dx} \sim \left(\frac{dF}{dt}\right)\left(\frac{1}{U_c}\right) \sim \left(\frac{dF}{d(t/t_0)}\right) . \tag{43}$$

Figure 11 shows these diagnostics for several convective Mach number as a function of t/t_0. For the two lowest values of M_c, 0.3 and 0.6, the mixing efficiencies are very close. As M_c increases, there is a delay in the onset of the convective-mixing regime, as shown in M_Y and $M_{\nabla Y}$. This can be understood by noting that an increase in M_c changes the amplification rates of the first excited modes[10]. A further increase in M_c results in a decrease in the efficiency of mixing, as shown for 0.9 and especially notable for 1.2. The growth of M_X is reduced by over a factor of two by increasing M_c from 0.6 to 1.2, which shows a well known trend of compressibility. The experimental reduction factor is even larger for a supersonic single-species mixing layer, almost a factor of four.[2,3] Previous numerical results[13,14] that used the thickness of the vorticity to characterize the mixing efficiency (a parameter which is similar to M_X), show the same trends. Figure 12, the instantaneous pressure and $Y_{H_2}(1 - Y_{H_2})$ for the computation with $M_c = 1.2$, shows the presence of shocks in the thin vortex layer. At these higher values of M_c, the structure not only shows the main mode, but also the growth of high-frequency secondary modes.[9] This behavior is characteristic of supersonic convective Mach numbers and explains many of the small structures seen in the spatial simulations.[17,18]

The Effect of Confining Boundaries

We first consider the effects of the finite size and periodicity of the computational domain by comparing computations for the same value of M_c and Δx, but with varying values of L (and therefore H). The right and left boundaries of the computations are still periodic, but the absolute size of the perturbing wavelength is the same, so that there are more wavelengths in the larger domain and fewer in the smaller. We now examine to what extent we can say that the smaller computation is a "piece" of the larger one.

The boundary condition seems to affect the convective mixing more than the diffusive mixing. Figure 13 shows the instantaneous scalar dissipation in the diffusive-mixing regime two cases, one with $L = 1$ cm and the second with $L = 0.5$ cm. The width and density of the structures are very similar. We also find that the absolute time to transition between the diffusive-mixing and convective-mixing stages increases with the size of the system, but normalized time in terms of t_0 does not vary.

However, there are effects of the confinement and periodicity on the flow that can be observed in the very late evolution of the flow when the mixture is almost homogeneous. Figure 14 shows that the periodicity and boundaries force the flow at acoustic frequencies typical of a confined chamber, shown in the graph of M_ω. The instantaneous contours marked 1, 2, and 3 are taken from those time marked similarly on the graph and show the flow at different time in its periodicity. Increased M_ω indicates increased dissipation of large vortices by viscosity. The fluctuations in M_ω superimposed on this general trend of increasing value, indicate oscillations between two quasi-stable states. One state is one large vortex, as shown in the Figure 16-1. This structure is broken up and the system reaches another stable state of several smaller vortices through the effects of the boundaries, as shown in Figure 16-3. The acoustic effects of boundaries for fast, subsonic, confined flows has been discussed extensively.[26]

The Dissipation Scale in the Diffusive-Mixing Regime

Because there are several dissipative processes present (viscosity, molecular diffusion, thermal conduction), it is important to determine what scales have to be resolved to simulate molecular mixing. To address this, we performed a series of computations where we successivly decreased the minimum dissipation scales computed by increasing the numerical resolution. The smallest scale present can be estimated as three times Δx for algorithms such as FCT. Therefore, in a series of computations we kept the value of M_c and L constant

and changed the number of computational cells in each direction while keeping the initial thickness δ_o the same.

The global mixing quantities showed that the durations of the laminar and mixing regimes do not change as the resolution is changed. In particular, we observed that the transition between the laminar growth and convective-mixing regime always occurred at the same normalized time. Some differences were observed for the two measurements of the mixing intensity, M_ω and $M_{\nabla Y}$, in that the level of mixing is underestimated when the resolution is too low. However, for resolution on the order of η_Y and up to factors of at least thirty greater than η_k, the mixing diagnostics M_X and M_Y converge quickly and show no significant changes as resolution increases: the mixing efficiency is computed to within 10% of what would be obtained by resolving every scale down to η_k. These tests are discussed in more depth in detailed discussions of the numerical issues in the computations.[29] This numerical result for two-dimensional mixig tends to confirm experimental observations[30,31] indicating that the thickness of mixing layers in turbulent flows are on the order of the Taylor scale, that is, η_Y.

Summary and Conclusion

In this paper, we examined the evolution of a two-dimensional, supersonic, confined shear layer with molecular hydrogen gas on one side and molecular oxygen gas on the other. The purpose of these simulations was to examine the importance of various diffusion processes (viscosity, thermal conduction, and molecular diffusion) on the mixing process, and to determine the extent to which compressibility affects the development of the layer. To look at these questions, we solved the full set of time-dependent Navier-Stokes equations with thermal conduction and molecular diffusion in addition to convection and viscosity.

The first problem encountered was how to initialize such a two-dimensional shear layer. Whereas there is an analytic similarity solution that gives the initial conditions for an incompressible shear layer with the same material on either side, there was no such solution for the highly compressible shear layer between different gases. Our approach was to solve an equivalent one-dimensional problem that was allowed to go to steady state and use this to initialize the two-dimensional problem. In a series of such one-dimensional tests, we first considered a low-velocity shear layer between the same materials and for which there was an initial discontinuity in the density and velocity, but the pressure and temperature were constant across the shear layer. As this problem evolved, it reached

a steady level corresponding to a similarity solution describing the system variables, a property previously noted by Sandham and Reynolds[13] for the case of a shear layer with the *same* material in both streams. Then the initial conditions for the two-dimensional problem were obtained by extending this approach to high-velocity flows between different streams of materials, including the effects of molecular diffusion and thermal conduction. A new result of this work is that these conditions also produce converged, self-similar solutions for finite-thickness compressible shear layers between different density gases.

A notable result of the simulations of two-dimensional, supersonic flow ($M_c = 0.6$ and higher) was the distinct appearance of three very different regimes in the flow:

1. The initially unstable laminar stage in which the structures grow as a consequence of the initial perturbation, but appear very ordered.
2. The convective-mixing regime, in which the vortices begin to interact with each other and mixing occurs as these structures merge and grow, is the entrainment stage.
3. The diffusive-mixing regime in which the large structures break down and molecular diffusion dominates.

The existence as well as selected global and local properties of these regimes was clarified by comparing various instantaneous and global averages of a number of system variables. For example, while the instantaneous contours of Y_{H_2} (for example, Figure 6) or X_{H_2} provide a qualitative description of the difference in the regimes, the global averages of $Y_{H_2}(1-Y_{H_2})$ or $X_{H_2}(1-X_{H_2})$ as a function of time (for example, Figures 5 or 9) provide a more quantitative measure. Specifically, M_Y and $M_{\nabla Y}$ peak near the transition from the convective-mixing to diffusive-mixing stages, but M_X increases monotonically. In addition, the duration of the diffusive-mixing and convective-mixing regimes were comparable or the flows studies. The transition between the two mixing stages does not depend on the Reynolds or the Peclet numbers and this transition occurs at the same dimensionless time for all three cases, indicating that it is only a function of the large-scale convection time scale, $t_0 = H/\Delta U$.

For a better understanding of the effects of diffusion in these various regimes, we varied the strength of binary diffusion parametrically by comparing cases in which it was turned off completely, kept at its physical value, and doubled. These tests showed that through the initial laminar stage, the properties are strongly affected by diffusion, and it is the end of this stage that sets the initial conditions for the convective-mixing stage. However, the convective-mixing process itself is very strong, and quickly erases any memory of its initial

conditions. In the final, diffusive-mixing stage, diffusion dominates the mixing process by dissipating the scalar energy through thin, turbulent layers whose width is on the order of the Taylor microscale. Thus we find that the diffusion effects are of primary importance in the first and last stages, and relatively important in the convective mixing stage.

One result of these computations is that they agree with the recently proposed idea that it may not be necessary to resolve all scales down to the Kolmogorov scale to describe the final mixing process.[7,30,31] The analysis of experiments by Miller and Dimotakis[30] suggested that the resolution requirement for looking at local mixing properties is about 25 time the Kolmogorov scale. In our numerical computations, a similar trend can be seen and explained by observing that the molecular mixing is achieved through mixing layers whose thickness δ_i is on the order of the Taylor scale and an order of magnitude larger than the Kolmogorov or Batchelor scales. In addition, we have effects of other physically diffusive processes (in addition to viscosity and convection) that could have an effect. However, the exact determination of mixing intensity requires us to compute the total density l_i of small-scale mixing structures and therefore to resolve the entire spectrum.

Earlier studies of of spatially evolving two-dimensional compressible shear layers[17] indicated that for such supersonic flows, the system passed through the convective-mixing stage and quickly evolved into small scales that would be a diffusive-mixing stage. The presence or location of bounding side walls changed only the time of transition, not the fact that transition occurred. To examine the specific effect of compressibility on the mixing process, we parametrically varied the convective Mach number in the range 0.3 to 1.2. The result is that the three regimes are always present in the transition process, irrespective of the value of the convective Mach number. However, in terms of the reduced time, which is inherently a function of M_c, the onset of the convective-mixing regime is delayed as M_c is increased. This effect may be attributed to the changes in the amplification rates of the first excited modes.[10] Here we also see the well known effect of compressibility that the mixing efficiency is greatly decreased as M_c becomes large.

Finally, we examined the effects of system size on the time of transition from the convective-mixing to the diffusive-mixing stages. Here we considered a larger system with the same boundary conditions and initial perturbation at the same wavelength. Our conclusions were that the absolute time of transition increased, but the normalized time t_0 remained essentially the same. This result is consistent with the previous results that showed that the transition always occurs in compressible flows, but the wall does, to some

extent, effect the timing.[17] In addition, the presence of boundaries (the confinement and periodicity) can have a decided effect on the very late-time evolution of the system, when the mixture is almost homogeneous, by forcing the flow at acoustic frequencies typical of the chamber. It is sensitivity to the acoustic perturbations which is likely to be the key to understanding the instability that leads to the transition from convective to diffusive mixing.

There are several important as yet unstudied aspects of the types of flows that are described above. The first is how the general and specific results shown here change for a three-dimensional problem. To answer this, we are currently conducting equivalent simulations in three dimensions. These are by nature much more expensive and so we are using the results from the simulations presented here as a guide. Another major problem we have begun to address is the effect of chemical-energy release. Hydrogen and oxygen are highly reactive and perhaps too explosive to be practical for such a problem. However, we are now examining the effects of hydrogen-air reaction and mixing in such these idealized layers and in viatiated axisymmetric jets.[28]

Acknowledgments

This work is funded by the Office of Naval Research through the Naval Research Laboratory, Société Européenne de Propulsion (Vernon, France) and by Air Force Office of Scientific Research. The authors would like to acknowledge the conversations and help from Drs. J.P. Boris, G. Patnaik, K. Kailasanath, D.L. Book, F.F. Grinstein, M. Lefebvre, and R. Dahlburg.

References

[a] On leave from ONERA and sponsored by Société Européenne de Propulsion, France.

[1] G.L. Brown and A. Roshko, "On density effects and large structures in turbulent mixing layers," J. Fluid Mech. *64*, 775, 1974.

[2] D.W. Bogdanoff, "Compressibility effects in turbulent shear layers," AIAA J. *21*, 926 (1983).

[3] D. Papamoschou, and A. Roshko, "Observations of supersonic free shear layers," AIAA Paper 86-0162, American Institute of Aeronautics and Astronautics, Washington, DC, 1986.

[4] P.E. Dimotakis, AIAA Paper 89-0262, "Turbulent free shear layer mixing," American Institute of Aeronautics and Astronautics, Washington, DC, 1989.

[5] N.T. Clemens, M.G. Mungal, T. Berger, and U. Vandsburger, AIAA Paper 90-0500, "Visualization of the structure of the turbulent mixing layer under compressible conditions," American Institute of Aeronautics and Astronautics, Washington, DC, 1990.

[6] M. Samimy and G.S. Elliot, "Effects of the compressibility on the struce of free shear layer," AIAA Paper 88-3054, American Institute of Aeronautics and Astronautics, Washington, DC, 1988.

[7] W.J.A. Dahm and K.A. Buch, "High resolution three-dimensional spatio-temporal measurements of the conserved scalar field in turbulent shear flows," in *Turbulent Shear Flows*, vol. 7, Springer (New York), 1991.

[8] R.W. Metcalfe, S.A. Orszag, M.E. Brachet, S. Menon and J.J. Riley, "Secondary instability of a temporally growing mixing layer," J. Fluid Mech. *184* 207 (1987).

[9] S.A. Ragab and J.L. Wu, "Instabilities of supersonic shear flows," *AIAA Paper 90-0712*, American Institute of Aeronautics and Astronautics, Washington, DC, 1990.

[10] T.L. Jackson and C.E. Grosch, "Absolute/convective instabilities and the convective Mach number in a compressible mixing layer," ICASE Report 89-3, NASA Langley Research Center, Langley, VA, 1989.

[11] J.J. Riley and R.W. Metcalfe, "Direct numerical simulation of a perturd turbulent mixing layer," AIAA Paper 80-0274, American Institute of Aeronautics and Astronautics, Washington, DC, 1980.

[12] P.A. McMurtry, J.J. Riley, and R.W. Metcalfe, "Effects of heat release in the large-scale structure in turbulent mixing layers," J. of Fluid Mech. *199* 297 (1989).

[13] N.D. Sandham and W.C. Reynolds, "A numerical investigation of the compressible mixing layer," Stanford University Report TF-45, Department of Mechanical Engineering,

Stanford, CA, 1989.

[14] S.K. Lele, "Direct numerical simulation of compressible free shear flows", AIAA Paper 89-0374, American Institute of Aeronautics and Astronautics, Washington, DC, 1989.

[15] S.A. Ragab and S. Sheen, Large-eddy simulation of a mixing layer, AIAA Paper 91-0233, American Institute of Aeronautics and Astronautics, Washington, DC,1991.

[16] M.C. Soteriou, O.M. Knio, and A.F. Ghoniem, "Manipulation of the growth rate of a variable density, spatially developing mixing layer via external modulation," AIAA Paper 91-0081, American Institute of Aeronautics and Astronautics, Washington, DC, 1991.

[17] R. Guirguis, F.F. Grinstein, K. Kailasanath, E.S. Oran, J.P. Boris, and T.R. Young, "Mixing enhancement in supersonic shear layers," AIAA Paper 87-0373, American Institute of Aeronautics and Astronautics, Washington, 1987.

[18] B. Farouk, E.S. Oran, and K. Kailasanath, "Numerical simulations of the structure of supersonic shear layers" Phys. Fluids A *3*, 2786–2798 (1991); also NRL Memorandum Report 6667, Naval Research Laboratory, Washington, DC, 203, 1990.

[19] Oran, E.S., and J.P. Boris, *Numerical Simulation of Reactive Flow*, Elsevier, 1987.

[20] T.P. Coffee, J.M. Heimerl, "Transport algorithms for premixed laminar steady-state flames," Combust. Flame *43*, 273 (1981).

[21] J.P. Boris and D.L. Book, "Solution of convective equations by the method of Flux-Corrected Transport," Meth. Comput. Phys. *16*, 85 (1976).

[22] G. Patnaik, K.J. Laskey, K. Kailasanath, E.S. Oran, and T.A. Brun, "FLIC – A Numerical, Two-Dimensional Flame Model," NRL Memorandum Report 6555, Navl Research Laboratory, Washington, DC, 1989.

[23] G.K. Batchelor, "Computation of the energy spectrum in homogeneous two-dimensional turbulence," Phys. Fluids, Supplement II, 233 (1969).

[24] M. Lesieur, C. Staquet, P. Le Roy, P., and P. Compte, "The mixing layer and its coherence examined from the point of view of two-dimensional turbulence," J. Fluid Mech. *192*, 511 (1988).

[25] J.E. Broadwell and R.E. Breidenthal, "A simple model of mixing and chemical reaction in a turbulent shear layer," J. Fluid Mech. *125*, 397 (1982).

[26] Koochesfahani, M.M., and P.E. Dimotakis, *J. Fluid Mech.*, 170, 83–112, 1986.

[26] M.M. Koochesfahani and P.E. Dimotakis, "Mixing and chemical reactions in turbulent liquid mixing layers," J. Fluid Mech. *170*, 83 (1986).

[27] J.P. Boris, On large eddy simulation using subgrid turbulence models, in *Whither Tur-*

bulence? or Turbulence at the Crossroads, Lecture Notes in Physics No. 357, pp. 334, ed. J.L. Lumley, Springer, NY, 1990.

[28] P. Vuillermoz, E.S. Oran and K. Kailasanath, "Effect of Damköhler number on a supersonic reactive mixing layer," P. Vuillermoz, E.S. Oran and K. Kailasanath, AIAA Paper 92-0337, American Institute of Aeronautics and Astronautics, 1991; also "The effect of energy release on a supersonic reactive mixing layer," to appear, *Proceedings of the 24th Symposium (International) on Combustion*, The Combustion Institute, Pittsburgh, PA, 1992.

[29] P. Vuillermoz and E.S. Oran, Resolution requirements for computing compressible mixing layers, in preparation.

[30] P.L. Miller and P.E. Dimotakis, "Stochastic geometric properties of scalar interfaces in turbulent jets," Phys. Fluids A *3*, 168 (1991).

[31] J.E. Broadwell, "Large-scale structures and molecular mixing," Phys. Fluids A *3*, 1193, 1991.

Tables

Table 1. Coefficients for H_2/O_2 mixture ($T = 500$ K, $P = 3.5 \times 10^4$ Pa)

X_{H_2}	X_{O_2}	μ_m	λ_m	D_{12}	Pr	Sc	Le
1.0	0.0	1.24×10^{-5}	0.260	5.13×10^{-4}	0.696	1.436	2.065
0.0	1.0	2.98×10^{-5}	0.042	5.13×10^{-4}	0.638	0.215	0.338

Table 2. Estimations of Kolmogorov and mixing scales

$l(m)$	M_c	Re	$\eta_k(m)$	$\eta_Y(m)$
5×10^{-3}	0.6	1.85×10^4	3.1×10^{-6}	3.7×10^{-5}
5×10^{-3}	1.2	3.70×10^4	1.9×10^{-6}	2.6×10^{-5}

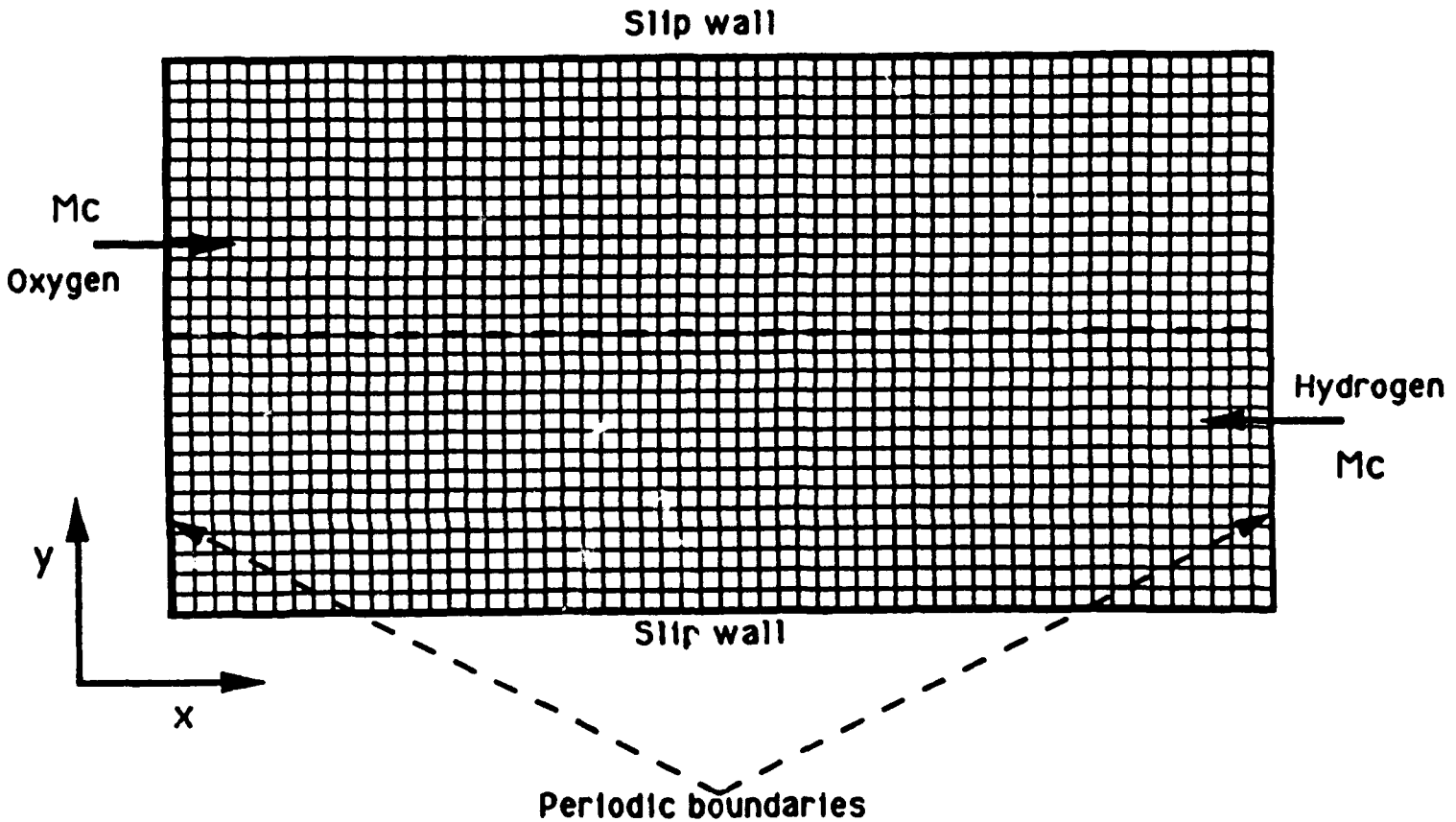

Figure 1. Schematic of computational domain for two-dimensional simulations.

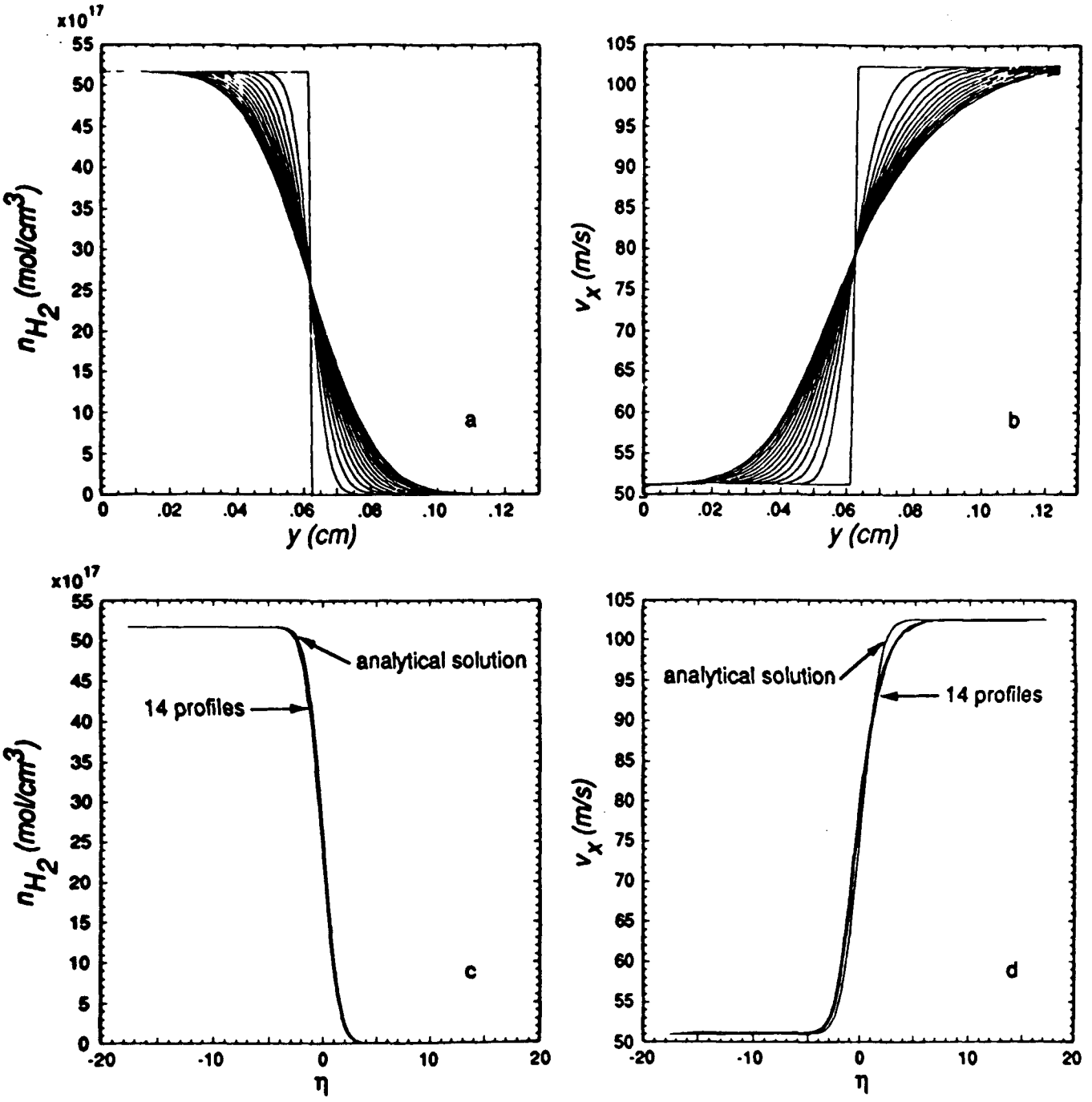

Figure 2. Computed and analytic similarity solutions for the one-dimensional mixing layer, M_c = 0.01, with hydrogen on both sides. Computed solutions for a) Number density of hydrogen, n_{H_2} and b) longitudinal velocity v_x as a function of the vertical coordinate y at successive times. Comparison of computed solutions (collapsed on the similarity variable η) and analytic solutions for c) n_{H_2} and d) v_x as a function of the vertical coordinate y.

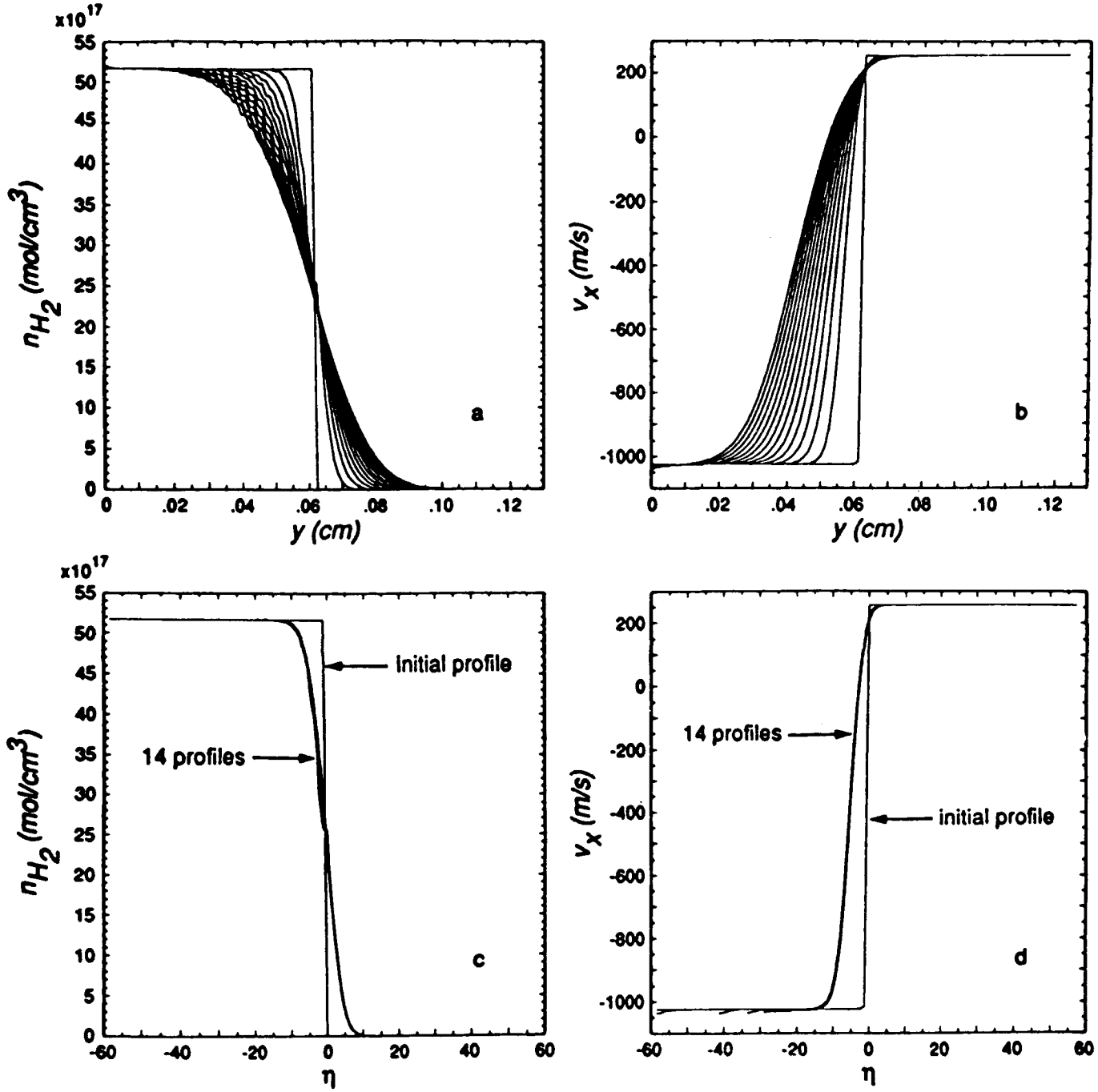

Figure 3. Computed one-dimensional solution for the hydrogen-oxygen mixing layer at successive times for $M_c = 0.6$. a) Number density of hydrogen, n_{H_2} and b) longitudinal velocity v_x, both as a function of the vertical coordinate y. c) and d) Collapsed profiles of the variables shown in a) and b) as a function of the similarity variable η.

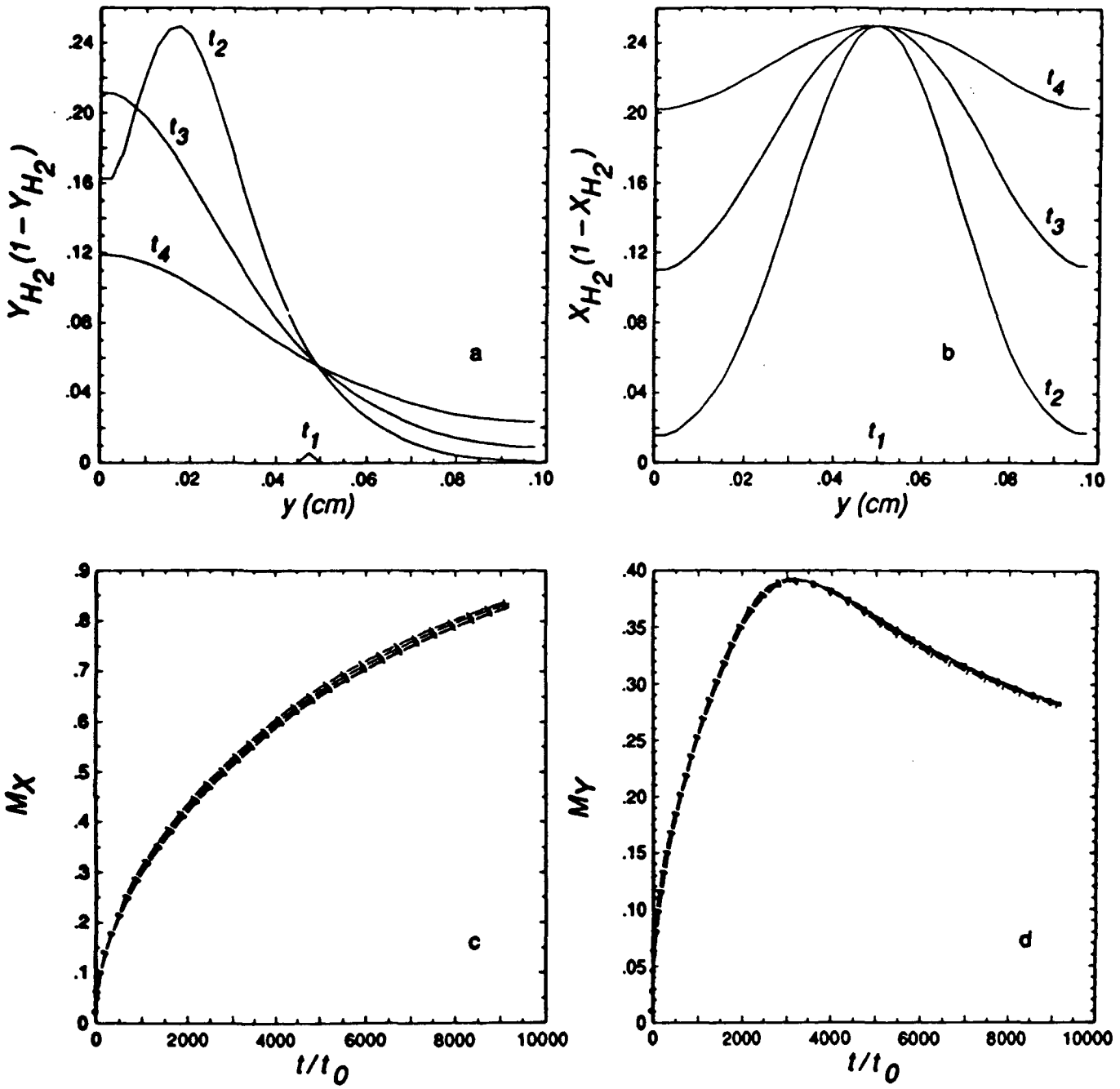

Figure 4. Computed mixing diagnostics for the one-dimensional hydrogen-oxygen shear layer at selected times as a function of vertical coordinate y at four selected times ranging from t_1 (close to $t = 0$) to late time, t_4. a) Longitudinal velocity v_x, and b) number density of hydrogen, n_{H_2}. Resolution tests showing the computed evolution of the global mixing parameters for the one-dimensional hydrogen-oxygen shear layer for four different resolutions and fixed system size. On each figure, curves marked "1" correspond to $N_x = 20$, $\Delta x = 10.0 \times 10^{-5}$ m, "2" to $N_x = 40$, $\Delta x = 5.0 \times 10^{-5}$ m, "3" to $N_x = 80$, $\Delta x = 2.5 \times 10^{-5}$ m, and "4" to $N_x = 160$, $\Delta x = 1.25 \times 10^{-5}$ m. c) M_X (equations (21)–(23)), and d) M_Y (equations (21)–(23)). Time is normalized by $t_0 = 0.5L/\Delta U$.

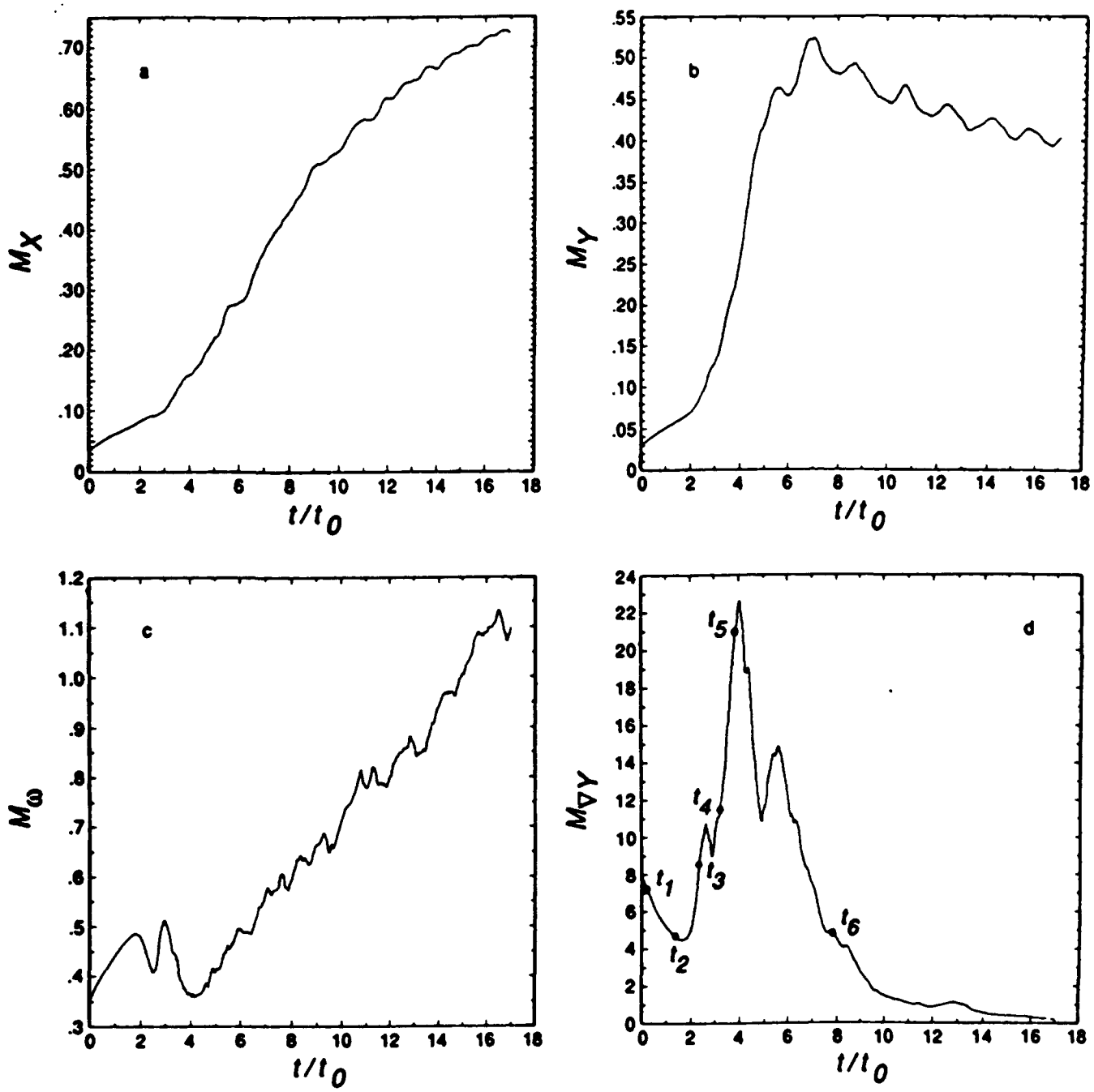

Figure 5. Global diagnostic parameters as a function of time for the two-dimensional hydrogen-oxygen shear layer computed with the NS+ equations (equations (3)–(18)) for $M_c = 0.6$, grid 200×100, and $\Delta x = 5.0 \times 10^{-5}$ m. a) M_X, b) M_Y, c) M_ω, and $M_{\nabla Y}$ (equation (27)).

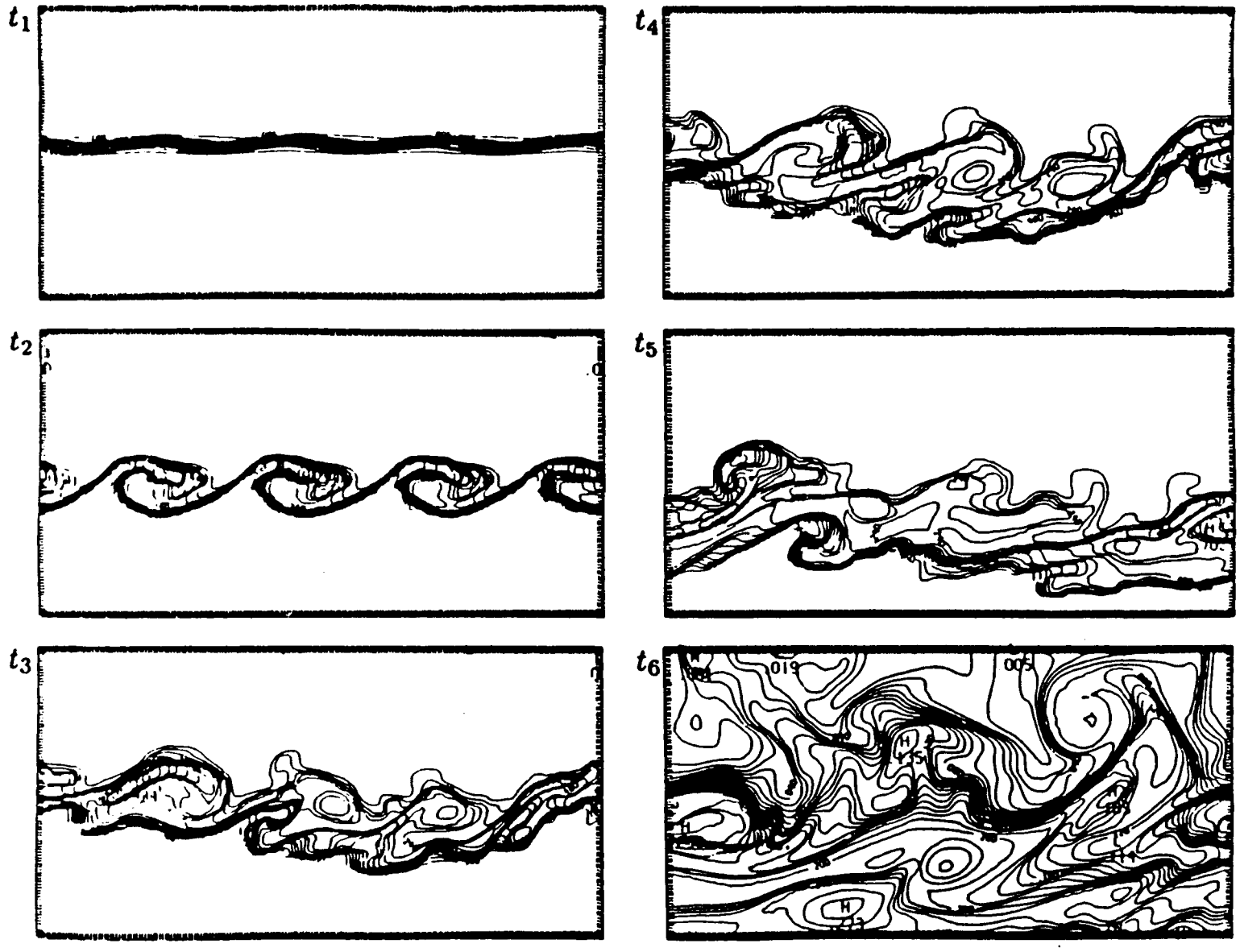

Figure 6. Instantaneous contours of Y_{H_2} for a sequence of six times for the computation described in Figure 5.

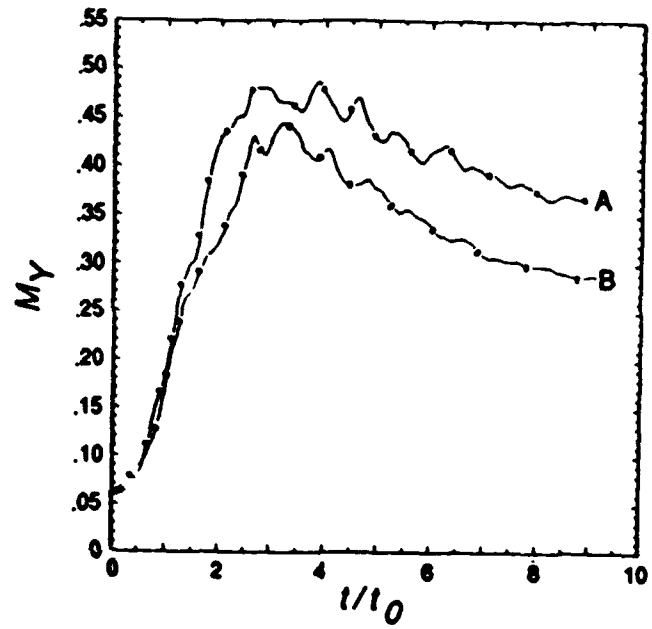

Figure 7. Comparison of M_Y for the Euler (A) and NS+ (B) solutions of the hydrogen-oxygen shear layer with $M_c = 0.6$, $T_1 = T_2 = 500\ K$, and grid 100×50, for $\Delta x = 0.5 \times 10^{-4}$ m, where $t_0 = 0.5L/\Delta U$.

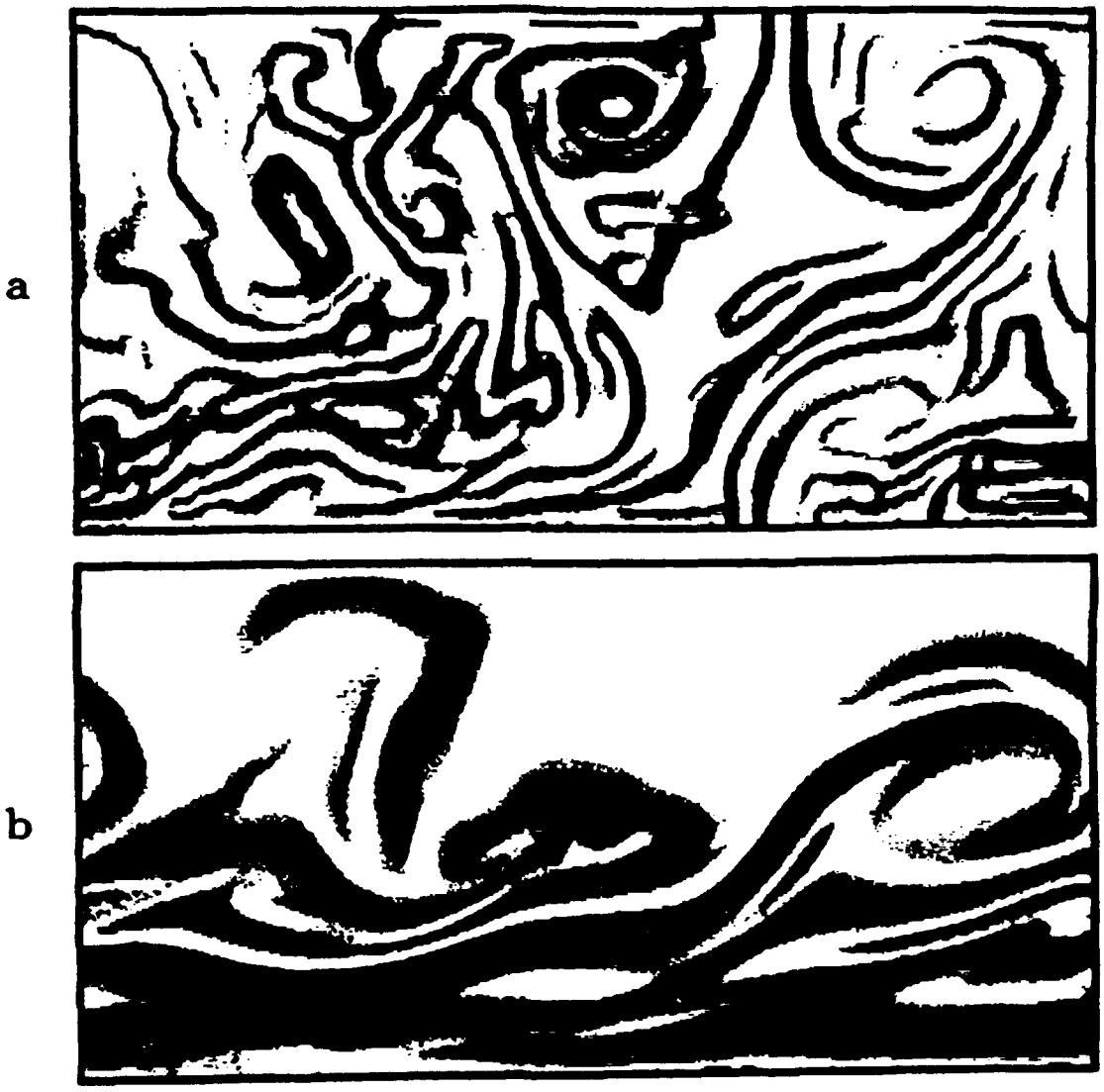

Figure 8. Instantaneous contours of the scalar energy dissipation, $(\nabla Y_{H_2})^2$ for the Euler and NS+ calculations with $\Delta x = 2.5 \times 10^{-5}$ m. Note that the palette is logarithmic.

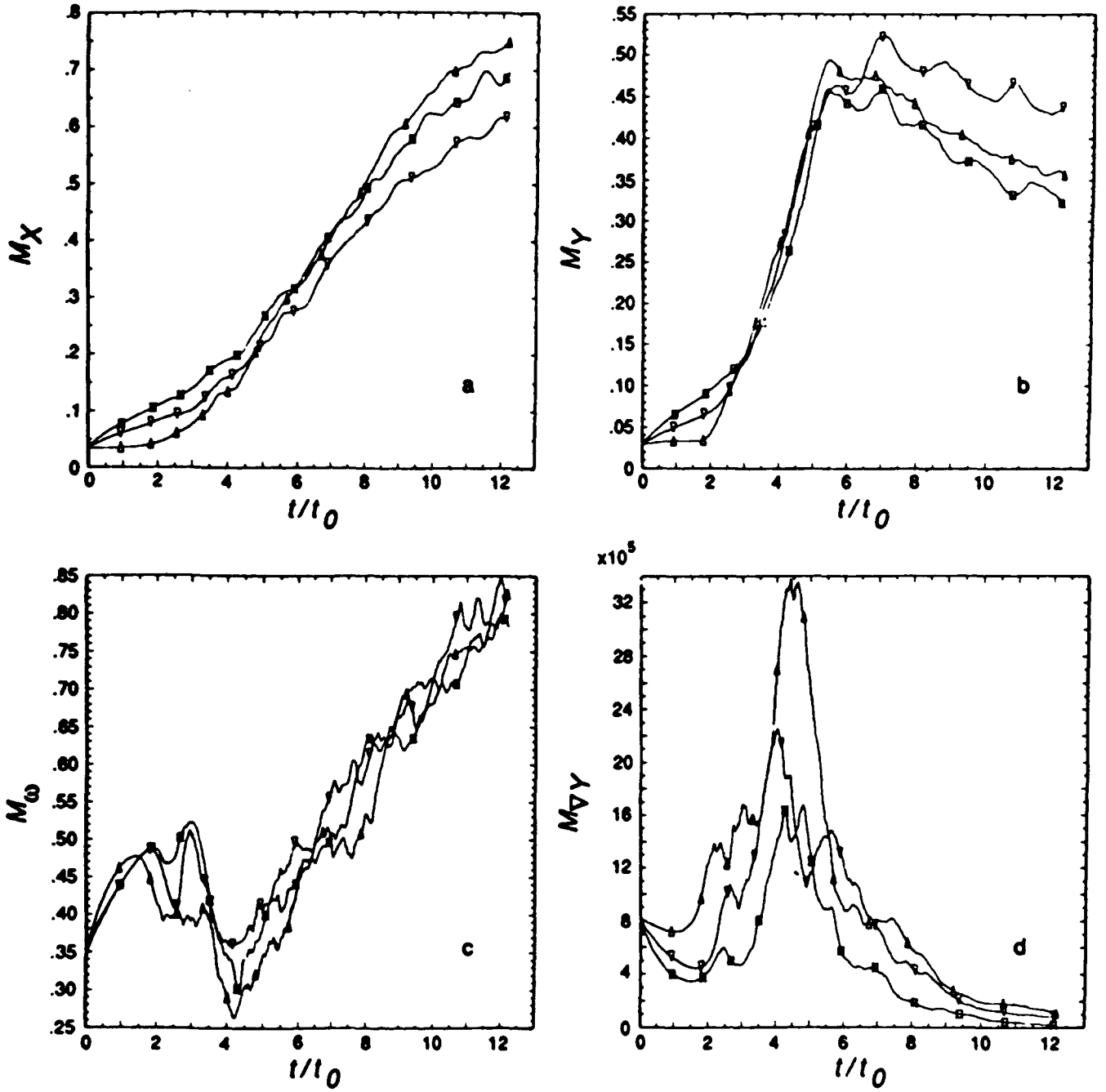

Figure 9. Evolution of the global mixing parameters for different molecular diffusion coefficients used in the NS+ equations: Δ = no molecular diffusion; ∇ = physical value; $\square$ = twice the physical value. a) M_X, b) M_Y, c) M_ω, d) $M_{\nabla Y}$.

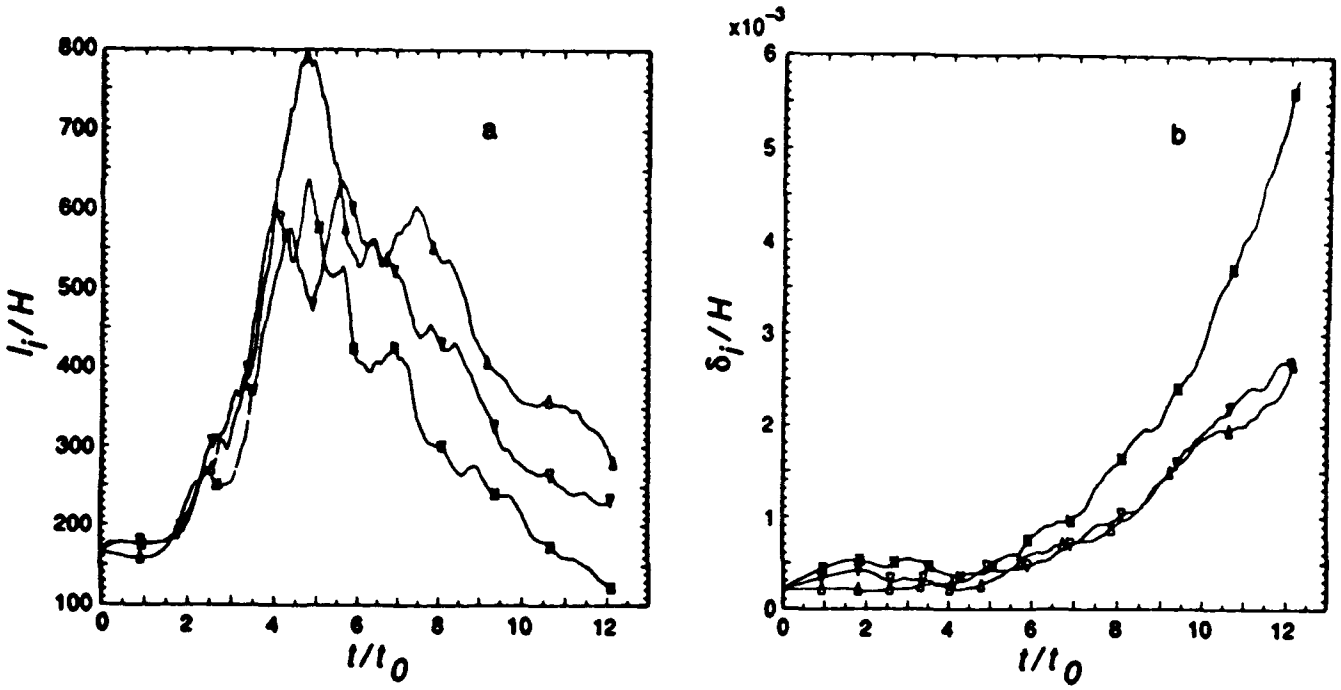

Figure 10. Evolution of a) the interface length, l_i, and b) interface width, δ_i, obtained from computations producing Figure 9, to evaluate the effects of molecular diffusion. Specific diffusion coefficients are marked as in Figure 9: Δ = no molecular diffusion; ∇ = physical value; $\square$ = twice the physical value.

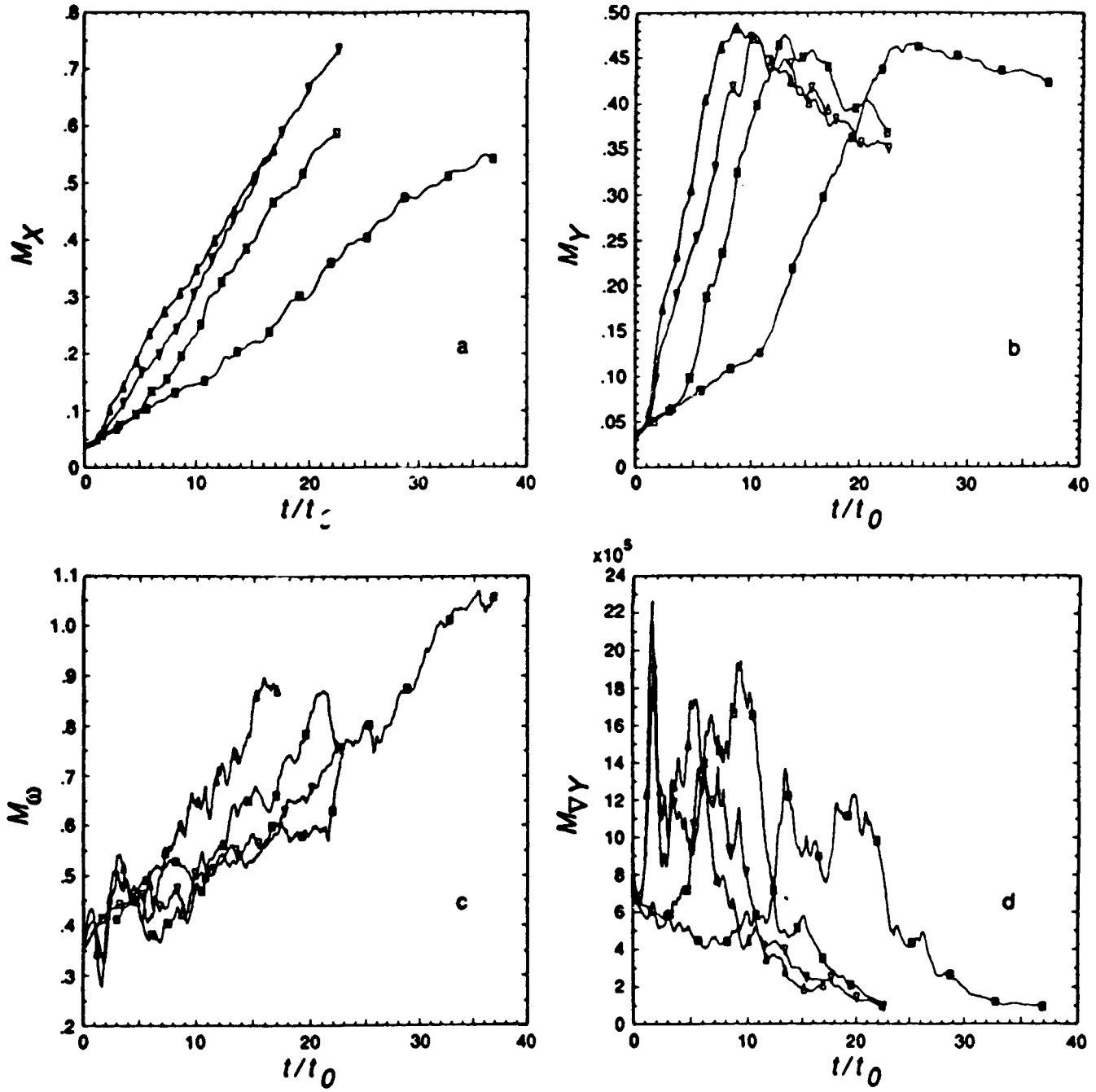

Figure 11. Evolution of the global mixing parameters for a $L = 1.0$ cm system, 200 × 100 grid, to show the effect of varying M_c: $M_c = 0.3$ marked by $\triangle$, $M_c = 0.6$ marked by ∇, $M_c = 0.9$ marked by ■, $M_c = 1.2$ marked by ■. a) M_X, b) M_Y, c) M_ω, and d) $M_{\nabla Y}$.

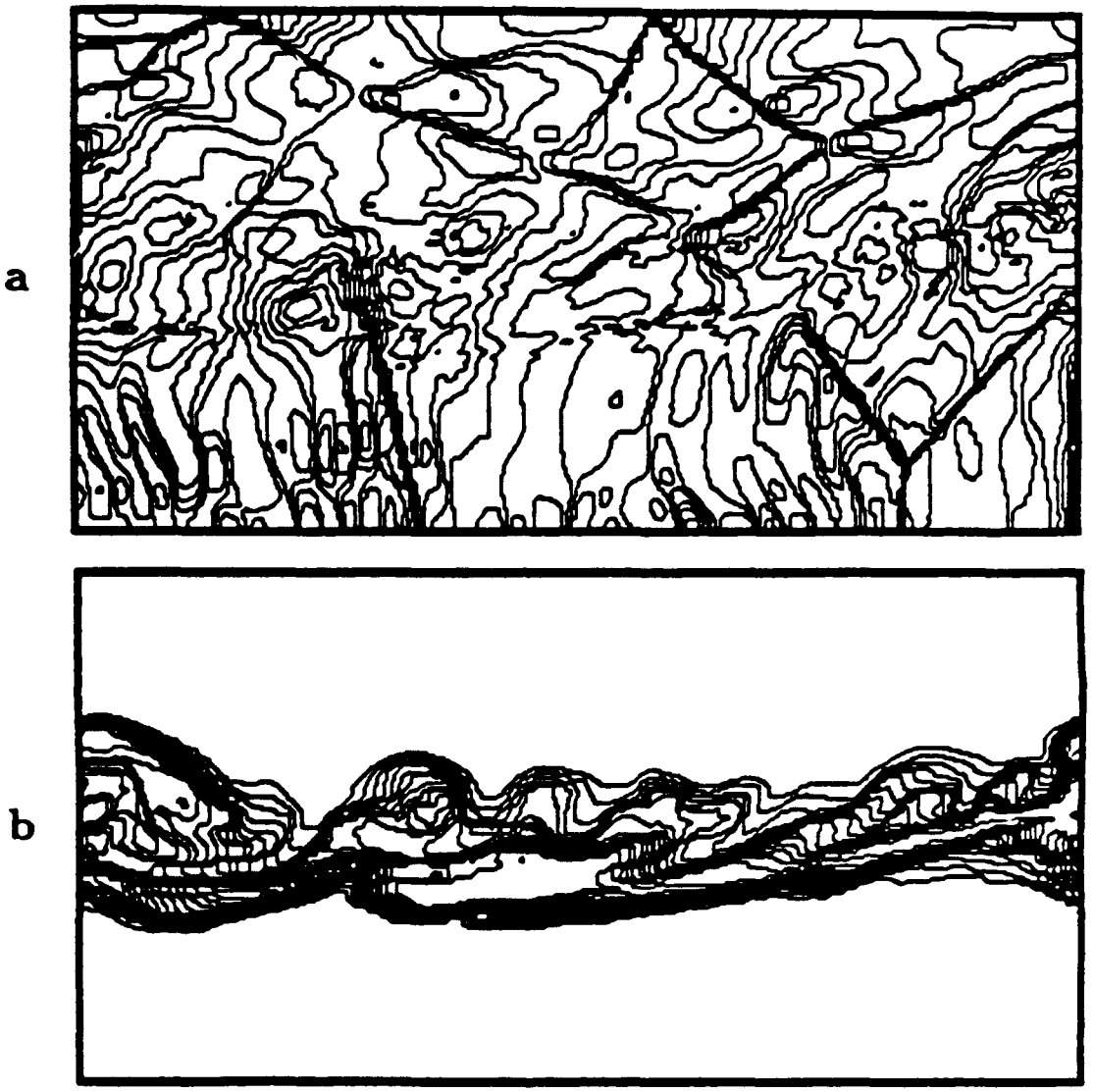

Figure 12. Instantaneous contours of a) pressure and b) $Y_{H_2}(1 - Y_{H_2})$ for $M_c = 1.2$, $L = 1.0$ cm, 200×100 grid.

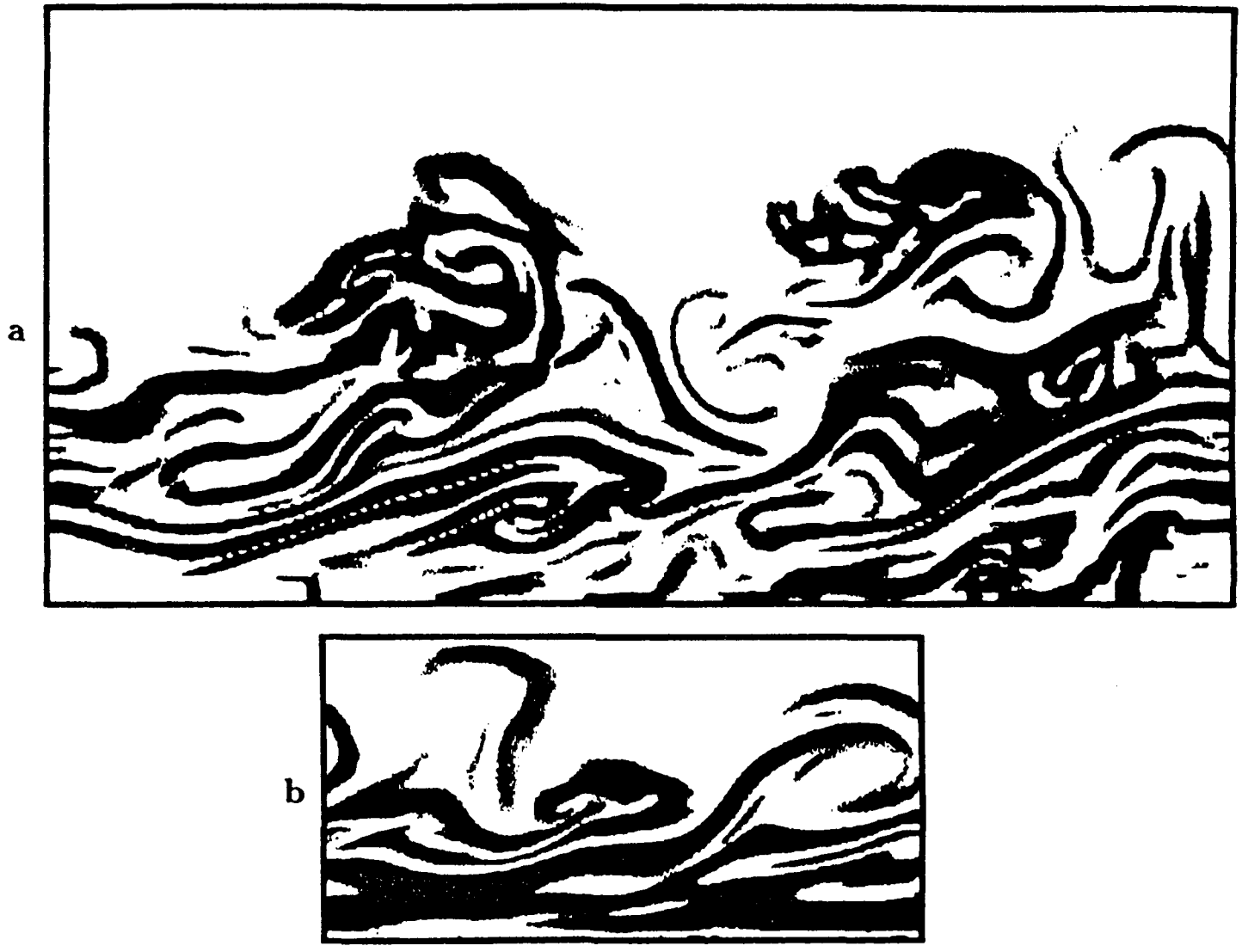

Figure 13. Instantaneous contours of the scalar energy dissipation $(\nabla Y_{H_2})^2$ for two computations showing the effects of the boundary conditions on the size of the structures in the diffusive-mixing regime: a) $L = 1.0$ cm, $\Delta x = 3.3 \times 10^{-5}$ m, initialized with a 4-wavelength harmonic disturbance; b) $L = 0.5$ cm, $\Delta x = 2.5 \times 10^{-5}$ m, initialized with a two-wavelength harmonic disturbance.

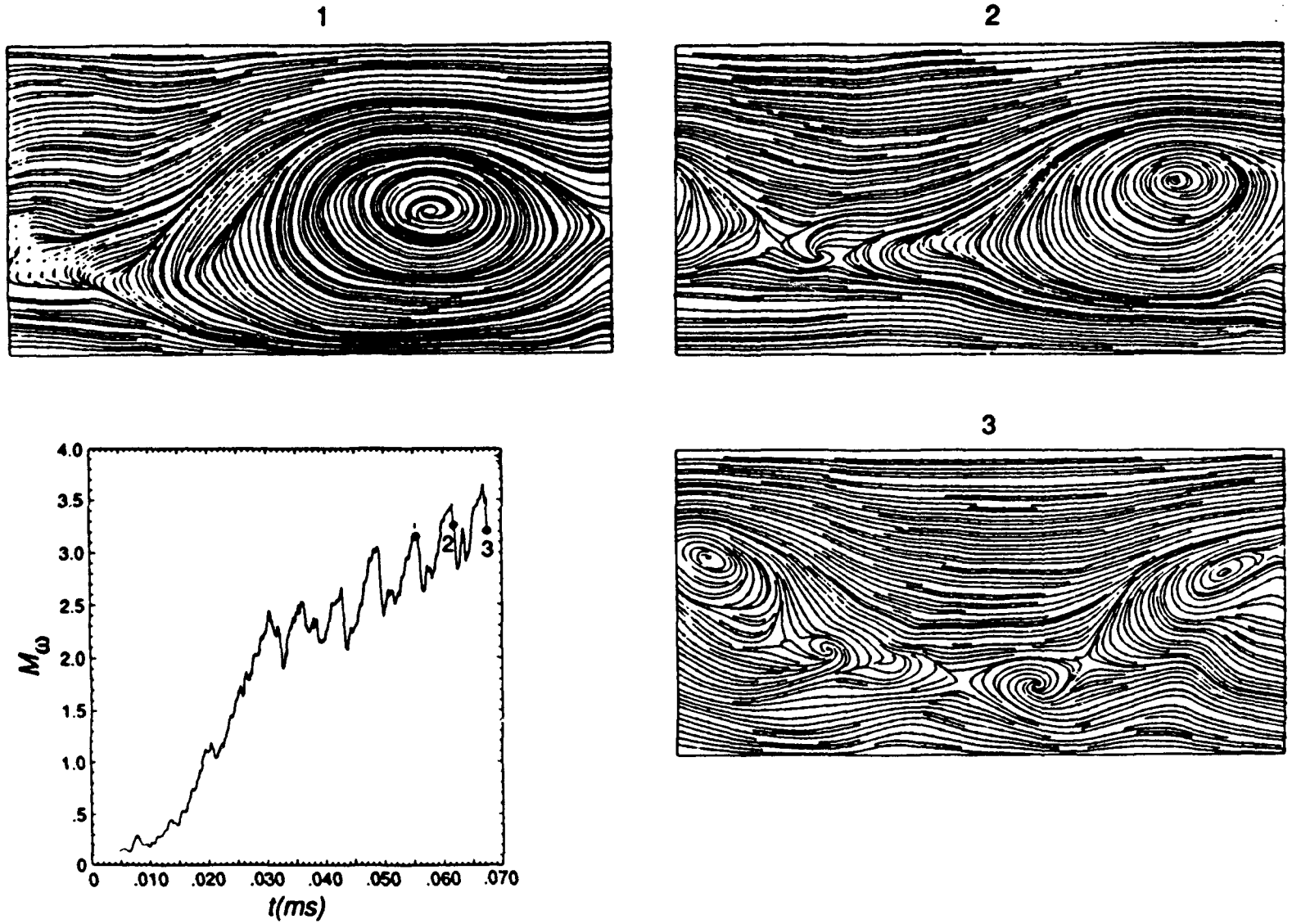

Figure 14. Effect of periodicity in the boundary conditions on the long-time evolution of the system. Figures marked 1, 2, and 3 indicate instantaneous streamlines at the times marked on the figure showing M_ω as a function of time.